International Journal of Science and Research (IJSR)
ISSN (Online): 2319-7064
Impact Factor (2012): 3.358

Applications of Numerical Simulation Method to Multistage Axial Flow Compressor Three-Dimensional Flow Field

Xuezeng Zhao[1], Xigui Wang [2], Yongmei Wang[3]

[1]Mechatronics School, Harbin Institute of Technology, Harbin 150001, China

[2]Mechatronics School, Harbin Institute of Technology, 703 Research of Institute, Harbin 150078, China

[3] Department of Motorcar Engineering, Heilongjiang Institute of Technology, Harbin 150036, China

Abstract: ***Numerical simulation method (NSM) has been developed as an important technique of computational inside fluid machinery complex blade tip clearance leakage flow. Clearance leakage and end wall boundary layer and the blade boundary layer interaction makes the tip clearance flow in showing 3D eddy current characteristics. Although the geometric size of blade tip clearance compared with the whole flow passage is very small, but it is on the blade passage nearly 20% regional flows, the tip leakage flow will result in the reduction of the tip near the work efficiency, resulting in channel blockage and local losses increase, therefore the correct prediction of the tip leakage flow phenomenon has important significance on further improve the performance of axial flow compressor rotor and expand the stable working range of the rotor.***

Keywords: Numerical simulation method, Axial flow compressor, Tip clearance, Tip leakage flow, 3D eddy current characteristics

1. Introduction

Numerical simulation method (NSM) has received considerable interest in the past decades as an efficient method of computing a variety of compressor and turbine cascades (Chen and Doolen, 1998; Filippova et al., 2001). Meanwhile, incorporated with corresponding models, it was applied to numerous interdisciplinary fieds, such as multiphase flow (Chen et al., 2011), natural convection (Scagliarini et al., 2010), etc. Early numerical simulation method is easy to determine the boundary conditions, has short computing time, less memory, but generally used to calculate the viscous flow field in 2D (Chen and Doolen, 1998). Three element flow theory of fluid machinery, the further development of a variety of S1 stream surface and S2 surface flow numerical simulation method, the design concepts and tools has become indispensable in many high performance turbine and compressor engineering (Chen et al., 2003). On the other hand, by introducing implicit residual smoothing, the stability of the method could be improved (Lallemand and luo, 2003). Using local time stepping and multigrid convergence acceleration; add two order artificial viscosity term improved shock capturing stability, adding four order artificial viscosity term to eliminate the high frequency error solution (Liu et al., 2012). In recent years, Premnath (2009) made a numerical simulation of two-dimensional Navier-Stokes equation on VKI cascade and T12 turbine nozzle blade, captured a clear shock and wake interference graph, surface pressure distribution of blade with experimental data. Reynolda-Averaged two-dimensional Navier-Stokes calculations (Filippova et al.,2001; Zhou et al., 2010) were implemented, which showed great success in turnulence predictions. By using the method of its improved, the widely used double equation turbulent low Reynolds number k- ε model and q-ε model are compared, the results show that the two models to calculate the fast convergence, small amount of calculation, turbulent boundary treatment is simple, is not sensitive to the initial flow field. Numerical simulation method rapid development of mechanical viscous fluid, laid a solid foundation for fluid dynamics which play a role in the compressor design and verification system (Yu et al., 2003).

2. Numerical Model and Methods

2.1 Turbulent Numerical Simulation Model

Turbulent numerical simulation reflects Reynolds time averaged coupled turbulent model to solve the three-dimensional turbulent Navier Stokes equation. The following Spalart-Allmaras turbulence model equations:

$$\frac{\partial}{\partial t}\left(\rho\tilde{v}\right)+\frac{\partial}{\partial x_i}\left(\rho\tilde{v}u_i\right)=G_v+\frac{1}{\sigma_{\tilde{v}}}\left\{\frac{\partial}{\partial x_j}\left[\left(\mu+\rho\tilde{v}\right)\frac{\partial\tilde{v}}{\partial x_j}\right]+C_{b2}\rho\left(\frac{\partial\tilde{v}}{\partial x_j}\right)^2\right\}-Y_v \quad (1)$$

Eddy viscosity coefficient corresponding to the u_i equation (1) working variables in $\tilde{v}$ (except for the near wall zone), eddy viscosity coefficient $\tilde{v}$ represents a fixed.

$$\mu_t=\rho\tilde{v}f_{v1} \quad (2)$$

f_{v1} is a viscous damping function,

$$f_{v1}=\frac{\chi^3}{\chi^3+C_{v1}^3} \quad (3)$$

Equation (3) $\chi\equiv\frac{\tilde{v}}{v}$

Equation (1) G_v is the production of the eddy viscosity coefficients.

$$G_v = G_{b1}\rho\left[S + \frac{\tilde{\gamma}}{K^2 d^2}\left(1 - \frac{\chi}{1+\chi f_{v1}}\right)\right]\tilde{\gamma} \quad (4)$$

Equation (4) is d away from the wall distance, S is the scalar form deformation tensor.

$$S = |\Omega_{ij}| + 2.0\min\left(0, |G_{ij}| - |S_{ij}|\right) \quad (5)$$

Equation (5) $|G_{ij}| = \sqrt{2\Omega_{ij}\Omega_{ij}}$

$$\Omega_{ij} = \frac{1}{2}\left(\frac{\partial u_i}{\partial x_j} - \frac{\partial u_j}{\partial x_i}\right) \quad (6)$$

$$|S_{ij}| = \sqrt{2S_{ij}S_{ij}}$$

$$S_{ij} = \frac{1}{2}\left(\frac{\partial u_i}{\partial x_j} + \frac{\partial u_j}{\partial x_i}\right) \quad (7)$$

Equation (1) Y_v is the diffusion coefficient of eddy viscosity

$$Y_v = G_{w1}\rho g\left(\frac{1+G_{w3}^6}{g^6 + G_{w3}^6}\right)^{\frac{1}{6}} \quad (8)$$

$$g = \frac{\tilde{\gamma}}{\tilde{s}K^2 d^2} + G_{w2}\left[\left(\frac{\tilde{\gamma}}{\tilde{s}K^2 d^2}\right)^6 - \frac{\tilde{\gamma}}{\tilde{s}K^2 d^2}\right] \quad (9)$$

K von K á RM á n constant, C_{b2} is constant, $\sigma_{\tilde{v}}$ is $\tilde{v}$ Prandtl constant, V is the molecular motion of viscous coefficient.

And the corresponding constants are:

$$C_{b1} = 0.1335, C_{b2} = 0.622, \sigma_{\tilde{v}} = \frac{2}{3}, C_{v1} = 7.1, C_{w1} = \frac{C_{b1}}{\kappa^2} + \frac{(1+C_{b2})}{\sigma_{\tilde{v}}}$$

$$C_{w2} = 0.3, C_{w3} = 2.0, \kappa = 0.4187$$

Spalart-Allmaras turbulence model with fast convergence and not easy to diverge, computing resource requirements.

2.2 Convergence Acceleration Techniques

Implicit residual smoothing is a weighted average value of adjacent point value to replace every bit of the residuals, this acceleration technique has become a standard technique for acceleration of steady numerical solution of convergence. Through the analysis of the model of the problem can be concluded: residual smoothing stability can extend the basic format, it can make the residuals obtained relatively large attenuation at every time step, and effectively dissipation error to the high-frequency component, eliminate numerical oscillation, so as to accelerate the convergence speed in order to accelerate the convergence, usually implicit residual smoothing technique with Runge-Kutta method in conjunction.

First use of central type of formula (10) on the residual R smoothing, in order to obtain the smoothing of the residual $\tilde{R}$.

$$U^{m+1} = U^n + a_m \Delta t F\left(U^m\right) = U^n + a_m R\left(U^m\right) \quad (10)$$

The fairing methods are as follows:

$$\left(I - \varepsilon_i \Delta_i^2\right)\left(I - \varepsilon_j \Delta_j^2\right)\left(I - \varepsilon_k \Delta_k^2\right)\tilde{R} = R \quad (11)$$

In equation (11) $\Delta_l^2\left(l = i, j, k\right)$ meet:

$$\Delta_l^2 \tilde{R} = \tilde{R}_{l-1} - 2\tilde{R}_l + \tilde{R}_{l+1}\left(l = i, j, k\right) \quad (12)$$

In equation (12) ε as a fairing factor, while satisfying equation (13) when calculating the stability:

$$\varepsilon > \frac{1}{4}\left[\left(\frac{\sigma^*}{\sigma}\right)^2 - 1\right] \quad (13)$$

σ^* and σ is the number of CFL residual smoothing after and smoothing before, according to equation (13), in the calculation can choose a larger σ^*, at the same time to adjust the ε value to ensure convergence.

2.3 Solid Wall Boundary Conditions

Calculation of 3D flow field in the fluid machinery, including the blade surface boundary, hub, gearbox. On the surface, the casing is motionless, the blade surface and the hub for rotation. Has a great influence on the surface boundary condition for numerical simulation of the flow field. In the setting of boundary conditions need to meet the following conditions:

1. On solid wall flow to meet impermeable, relative to the no slip condition.
2. Static object surface, the absolute velocity $\vec{C} = 0$.
3. Rotating surface, speed $\vec{W} = \omega r$, The sign of rotation speed in the Fine/Turbo by the right-hand rule decision. When the blade is to counter clockwise rotation, rotation speed is positive, and negative otherwise.

Absolute coordinate projection momentum equation along the surface normal direction $\vec{n}$:

$$\vec{n}\cdot\vec{\nabla}p = -\rho\vec{n}\cdot\left(\vec{V}\cdot\vec{\nabla}\right)\vec{V} + \vec{n}\left(\vec{\nabla}\cdot\vec{\tau}\right) \quad (14)$$

The pressure surface normal to the representation for the following form:

$$\vec{n}\cdot\vec{\nabla}p = \frac{1}{\left|\vec{S}_j\right|\Omega}\left(\vec{S}_j\cdot\vec{S}_i\frac{\partial p}{\partial\xi} + \vec{S}_j\cdot\vec{S}_j\frac{\partial p}{\partial\eta} + \vec{S}_j\cdot\vec{S}_k\frac{\partial p}{\partial\varsigma}\right) \quad (15)$$

In equation (15), ξ、η、ς are the coordinates I, J, K direction. Assume that J direction away from the wall (not necessarily vertical wall), $\vec{S}_i$、$\vec{S}_j$、$\vec{S}_k$ is the surface vector element.

By equation (14) and (15) available:

$$\frac{\partial p}{\partial \eta}=\frac{1}{\left|\vec{S}_j\right|^2}\left(\vec{S}_j\cdot\vec{S}_i\frac{\partial p}{\partial \xi}+\vec{S}_j\cdot\vec{S}_k\frac{\partial p}{\partial \varsigma}\right)-\frac{\Omega\rho}{\left|\vec{S}_j\right|}\vec{n}\cdot\left(\vec{V}\cdot\vec{\nabla}\right)\vec{V}+\frac{\Omega}{\left|\vec{S}_j\right|}\vec{n}\left(\vec{\nabla}\cdot\vec{\tau}\right)$$

（16）

By equation (16) by $\frac{\partial p}{\partial \eta}$ gradient pressure, static pressure on the wall can be determined by the equation (17):

$$P_w=P_1\frac{\partial P}{\partial \eta} \qquad (17)$$

In equation (17) W and 1 represent the wall surface and the first grid point

On the wall is adiabatic conditions, no heat exchange with the outside world, the wall temperature gradient is zero. Can get the following equation (18):

$$\frac{\partial T}{\partial \eta}=\frac{1}{\left|\vec{S}_j\right|^2}\left(\vec{S}_j\cdot\vec{S}_i\frac{\partial T}{\partial \xi}+\vec{S}_j\cdot\vec{S}_k\frac{\partial T}{\partial \varsigma}\right) \qquad (18)$$

The static temperature on the wall surface and the static pressure on the wall surface to determine the identifying similar:

$$T_w=T_1\frac{\partial T}{\partial \eta} \qquad (19)$$

Thus, the solid boundaries coincide with grid surface mass flux, momentum flux and energy flux is zero.

2.4 Periodic Boundary Conditions

Calculation of a blade passage as the computational domain. In leaves before and after the extension region on the boundary, motivated by physical considerations, must meet the periodic boundary conditions. Considering the flow parameters of periodic region boundaries in the flow field, the general selection of flow parameters of extraterritorial point value, using the same calculation method and interior point, obtained through periodic conditions. At the same time according to the periodic boundary conditions can be directly after the flow parameters on the border point of flow parameters as the front interface.

For the periodic condition of two stage compressor for: all row channel blades extending upstream and downstream section and tip clearance on the suction side and imposed periodic boundary condition; All the blade row channel extending upstream and downstream section and tip clearance of the pressure side and imposed periodic boundary condition.

3. Results and Discussions

3.1 The performance impact of axial flow compressor tip clearance

With the given parameter, based on the Numeca software, using the existing grid, axial flow compressor are calculated clearance and clearanceless grid. Blade tip clearance grid is shown in Fig.1

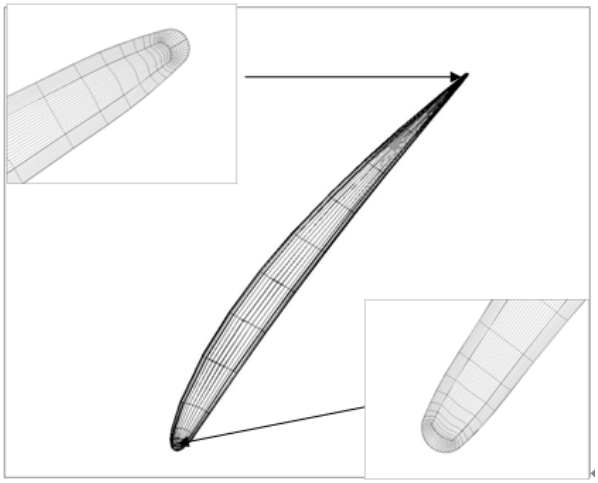

Figure 1: Blade tip clearance grid

The solvability condition of compressor design condition data (Listed in Table 1). With the aforementioned design point computational results data, clearance and clearanceless design conditions characteristic curve contrast. The corresponding efficiency and pressure radio and flow are shown in Fig.2.

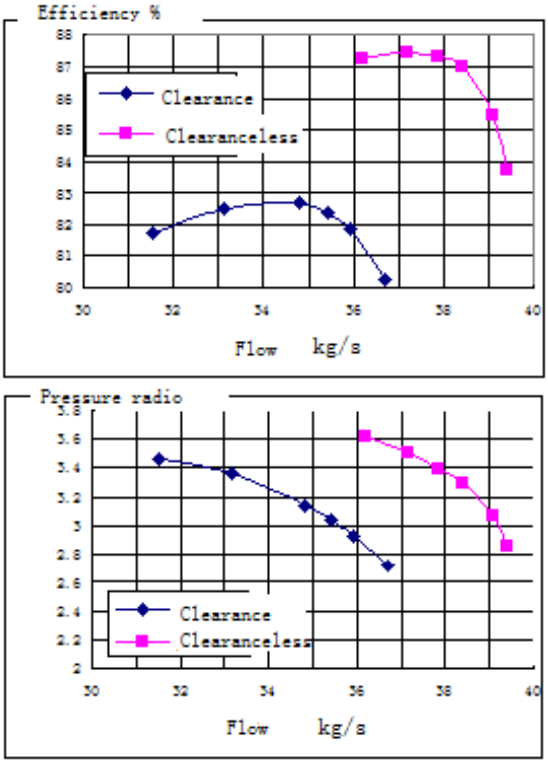

Figure 2: Clearance and clearanceless design conditions characteristic curve contrast

Table 1: The design point computational results data

D.P.	*Pressure radio*		*Flow(kg/s)*		*Efficiency(%)*		*Single step length (s)*		*Convergence step number*	
	Clearance	Clearanceless	Clearance	Clearanceless	Clearance	Clearanceless	Clearance	Clearanceless	Clearance	Clearanceless
	3.2531	3.5172	35.763	38.289	83.718	88.769	64	58	2200	1700

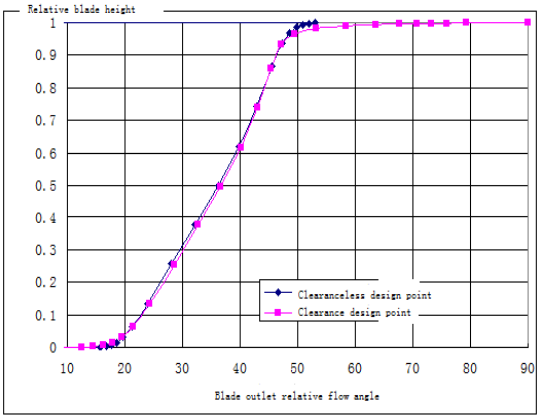

Figure 3: Second stage rotor blade outlet relative flow angle

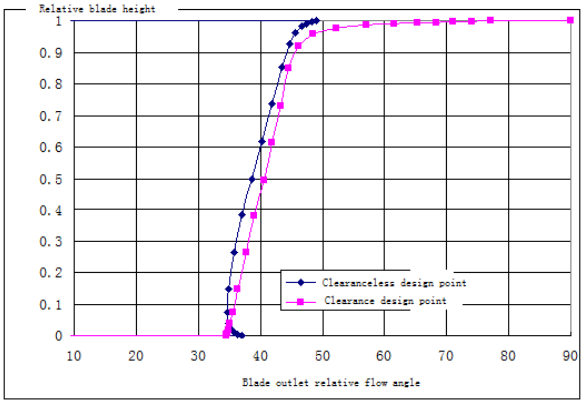

Figure 4: Sixth stage rotor blade outlet relative flow angle

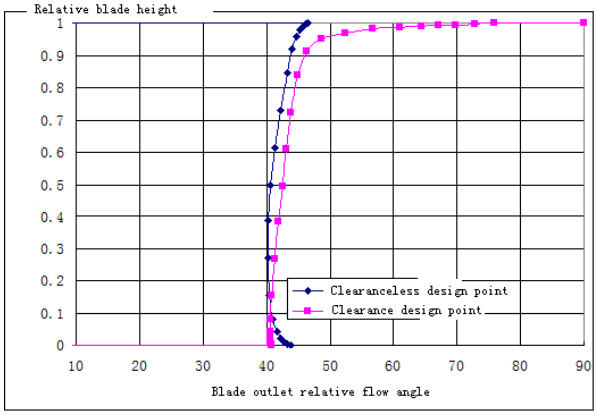

Figure 5: Eighth stage rotor blade outlet relative flow angle

At the speed of 5870r/min conditions, blade rotor circumferential average outlet relative flow angle distribution along the radial of the graph. As shown in figure 3-5.

From which can easily find, in the second stage rotor blade outlet angle in the 95% leaf high the following basic no change, but exports in leaves of 95% leaf high above the relative flow angle has certain change. With the influence of gap flow backwards, the cumulative increase gradually, the dynamic changes of blade outlet angle increases. This phenomenon is due to the pressure surface of blade to blade suction surface directly through the clearance leakage flow near the top of the air compressor rotor blade less deflection. In the vicinity of the rotor casing, because of the influence of casing in relative motion, so that the working ability of the compressor was significantly decreased, the pressure ratio and efficiency are reduced.

A tip clearance and no tip clearance, the Maher number and the static pressure contour of rotor blade section 50%, as shown in figure 6-13. Through the comparison we can see, both blade pressure surface and suction surface of blade, Maher distribution is obtained and did not consider the Maher number distribution when the gap and not much difference, it shows little effect on flow field in the rotor tip clearance flow in the middle part of the leaf.

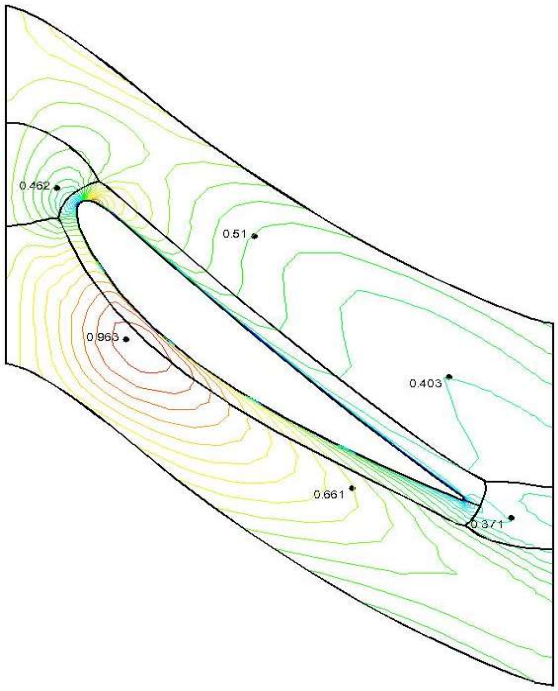

Figure 6: Clearanceless level 2 with 50% leaves high Maher number distribution

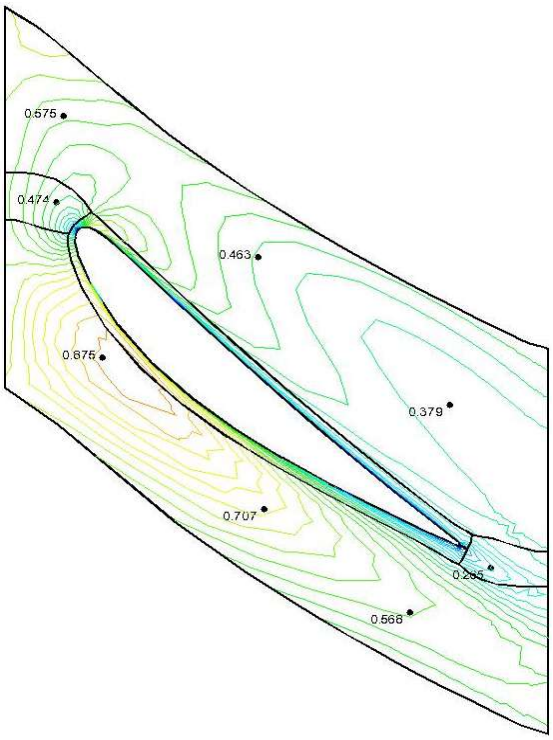

Figure 7: Clearance level 2 with 50% leaves high Maher number distribution

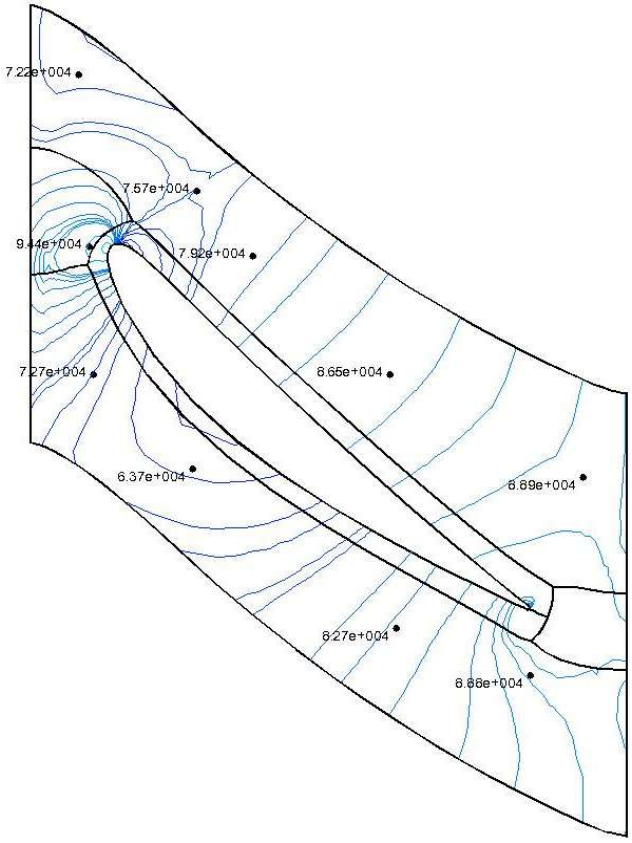

Figure 8: Clearanceless level 2 with 50% leaves high hydrostatic pressure distribution

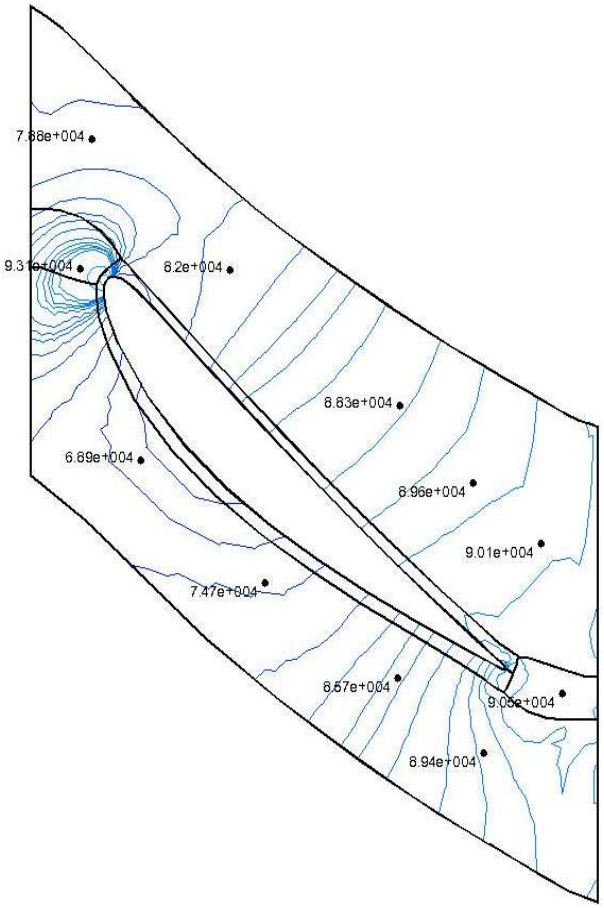

Figure 9: Clearance level 2 with 50% leaves high hydrostatic pressure distribution

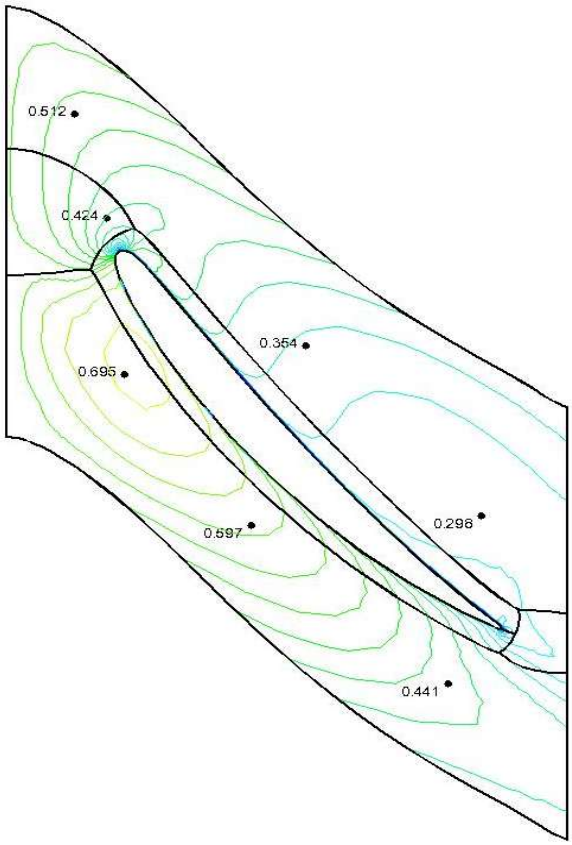

Figure 10: Clearanceless level 8 with 50% leaves high hydrostatic pressure distribution

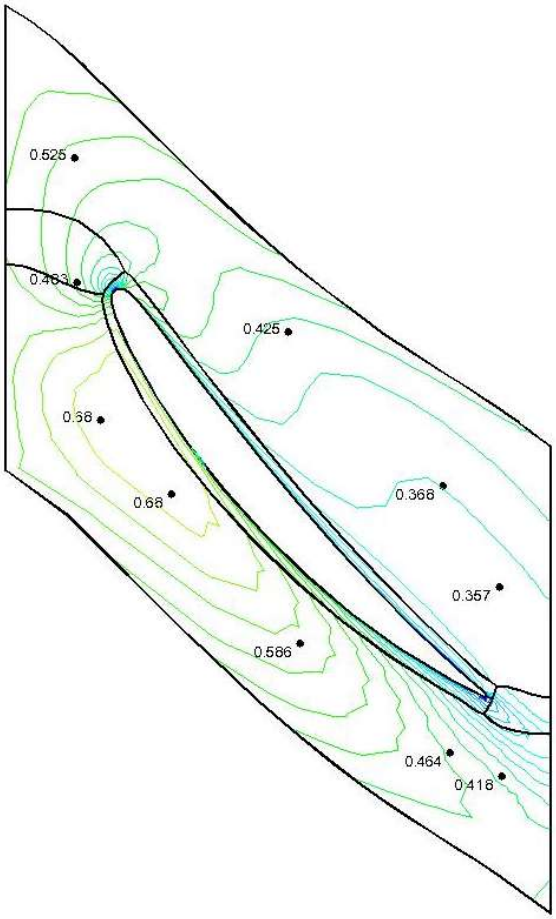

Figure 11: Clearance level 8 with 50% leaves high hydrostatic pressure distribution

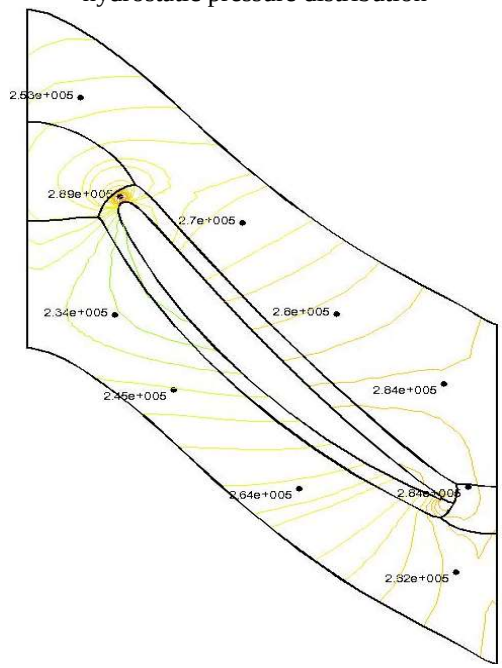

Figure 12: Clearanceless level 8 with 50% leaves high hydrostatic pressure distribution

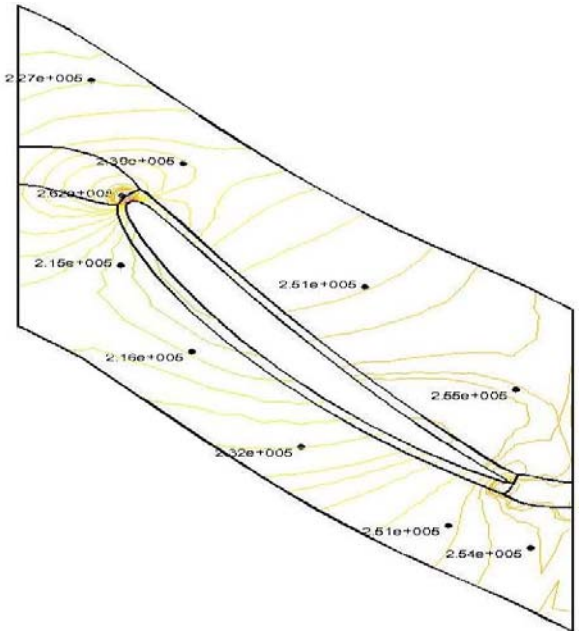

Figure 13: Clearance level 8 with 50% leaves high hydrostatic pressure distribution

A tip clearance and no tip clearance, the Maher number and the static pressure contour of rotor blade section 99%, as shown in figure 6-13. Through the comparison we can see, the static pressure and the Maher number distribution are very different, because of the influence of tip leakage vortex, resulting in pressure distribution and the middle leaf height significantly different. Load the blade tip at load is significantly less than the intermediate lobe height, suggesting that there is a gap exists when the leaves decreased work capacity.

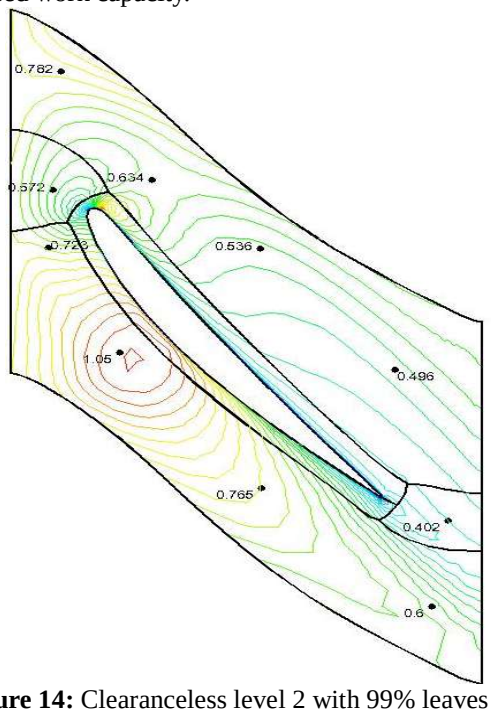

Figure 14: Clearanceless level 2 with 99% leaves high Maher number distribution

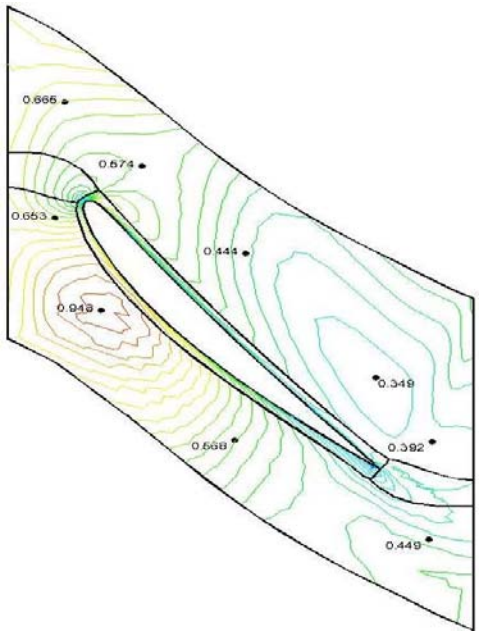

Figure 15: Clearance level 2 with 99% leaves high Maher number distribution

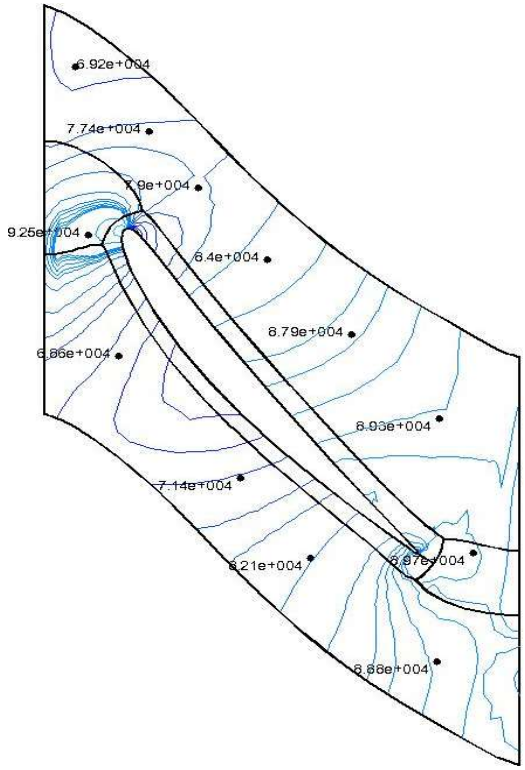

Figure 16: Clearanceless level 2 with 99% leaves high hydrostatic pressure distribution

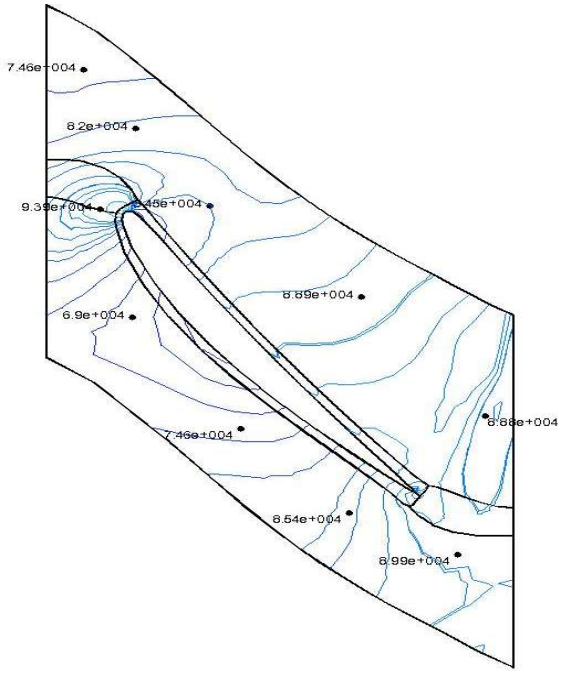

Figure 17: Clearance level 2 with 99% leaves high hydrostatic pressure distribution

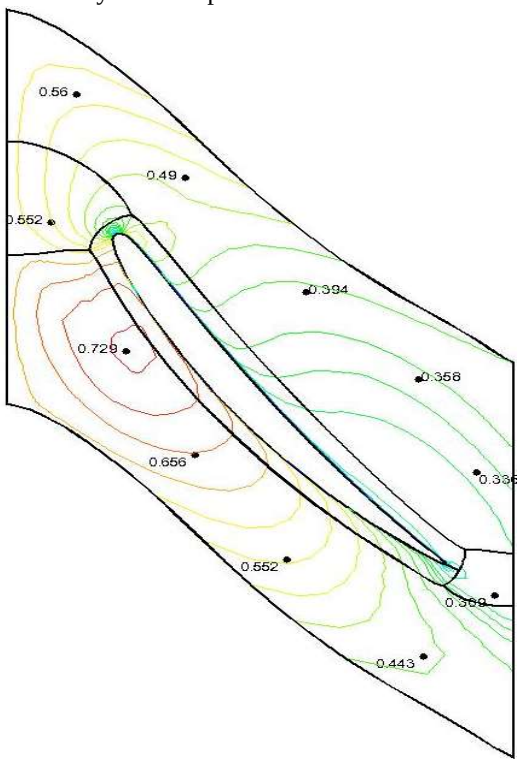

Figure 18: Clearanceless level 8 with 99% leaves high Maher number distribution

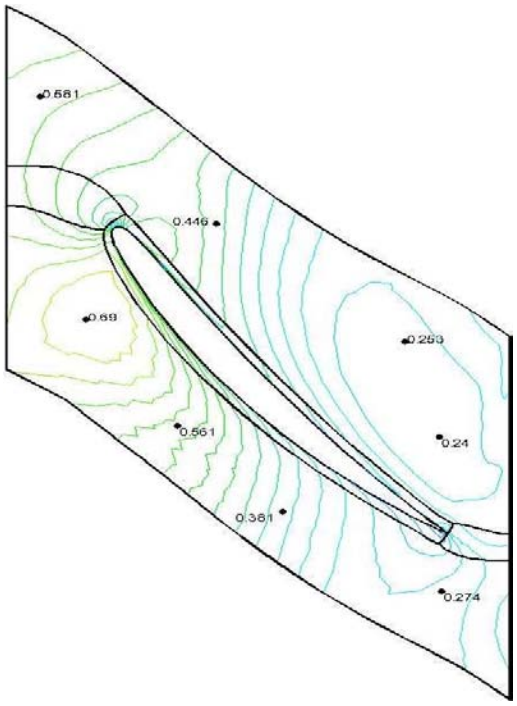

Figure 19: Clearance level 8 with 99% leaves high Maher number distribution

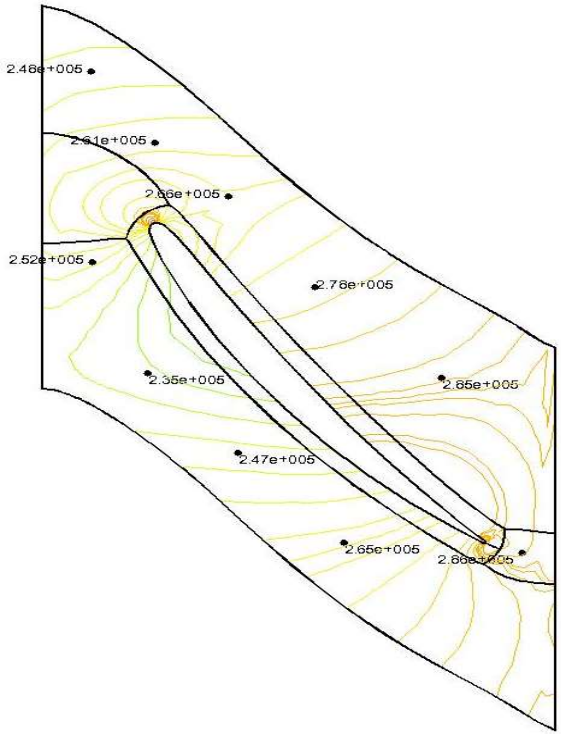

Figure 20: Clearanceless level 8 with 99% leaves high hydrostatic pressure distribution

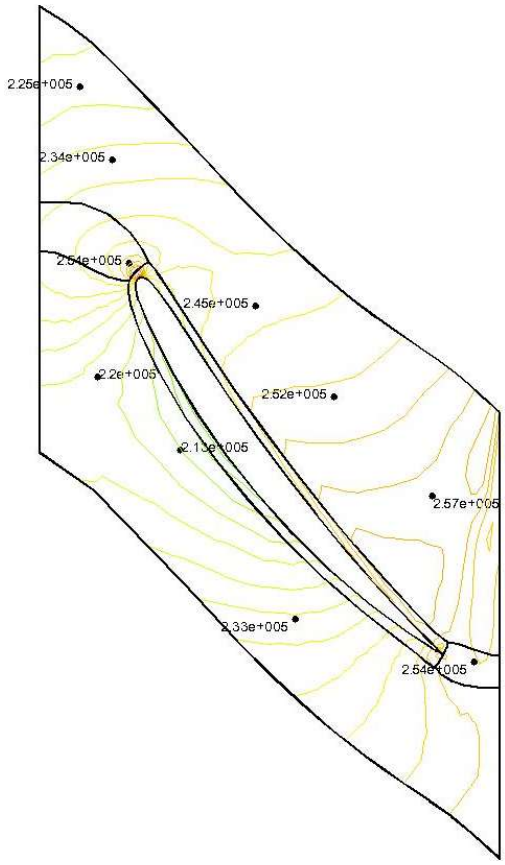

Figure 21: Clearance level 8 with 99% leaves high hydrostatic pressure distribution

3.2 Boundary layer transition effects on Performance

Influence of transition phenomenon affected by many parameters, among which the most important is the outflow surface characteristics of pressure distribution and the wall (roughness) and turbulence. In addition, the transition is an important part of the study of flow phenomena, which greatly affects the flow stress and heat transfer performance. In this paper, studies on transition issues are based on Numeca software.

When based on momentum thickness Reynolds number

$$R_{\theta s} = 163.0 + \exp\left[F(\lambda_\theta) - \frac{F(\lambda_\theta)}{6.91} T_u\right] \quad (20)$$

Then began a transition boundary layer.

Where: λ_θ is a dimensionless pressure gradient

$$\lambda_\theta = \frac{\theta^2}{\nu}\frac{dU_e}{ds} = \frac{\theta^2\left(\frac{\partial p}{\partial x}\right)}{\mu U_e}$$

U_e is outside the boundary layer boundary velocity, T_u is the turbulence intensity, S is the distance from the front along the flow direction, θ is momentum loss laminar thickness.

$$F(\lambda_\theta) = \begin{cases} 6.91 + 12.75\lambda_\theta + 63.64\lambda_\theta^2 & \lambda_\theta \le 0 \\ 6.91 + 2.48\lambda_\theta - 12.27\lambda_\theta^2 & \lambda_\theta > 0 \end{cases} \quad (21)$$

In this paper, the range: $-0.1 < \lambda_\theta < 0.1$, $0.3\% < T_u < 10\%$.

In this paper, the compressor at the design condition for the numerical simulation. The results are as follows:

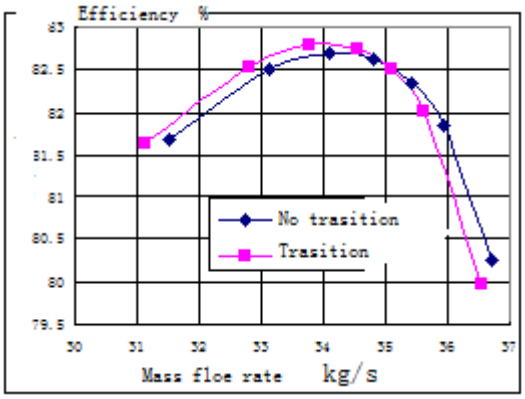

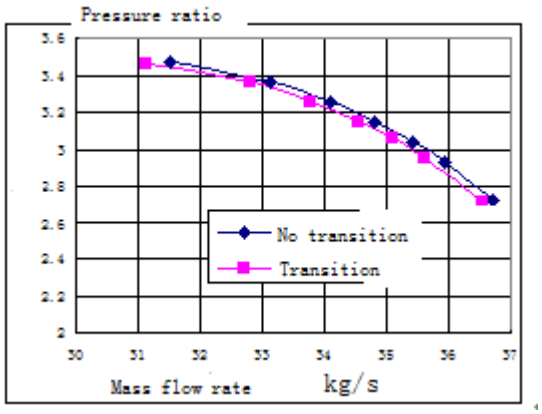

Figure 22: Join the boundary layer transition design operation characteristics curve comparison

Table 2: The design point computational results data

D.P	*Pressure radio*		*Flow(kg/s)*		*Efficiency (%)*		Single step length (s)		Convergence step number	
	Transition	No transition	Transition	No transition	Transition	No transition	Transition	No transition	Transition	No transition
	3.421	3.532	34.758	35.143	83.437	84.964	68	64	2900	2400

From Figure 22 we can see, the pressure ratio and efficiency in joined the transition model calculation basically no change. Description the Reynolds is larger, the transition has little effect.

4. Conclusions

In this study, tip leakage flows around axial flow compressor are simulated with numerical simulation methods coupled with turbulence model. Different computational aspects are discussed. The results are summarized as follows.

1. In relative coordinates conservation type Reynolds Navier-Stokes equation is given, and to introduce numerical computation discrete and accelerate the method of convergence.
2. Aiming at the blade tip clearance were calculated, draws the following conclusion: Clearance flow makes the rotor blade top outlet relative flow angle is changed greatly, which makes the work capacity of rotor drop, efficiency and pressure ratio decreased. Tip clearance flow directly affects the structure of flow field in the blade channels, increase the maelstrom, the deterioration of flow in compressor, reduces the scope of work. Tip clearance flow has great influence on rotor tip flow, but the effect on the flow field in the middle part of the small leaf.
3. According to the boundary layer transition were calculated, and comparison concluded: After adding transition, simulation of blade surface can better flow, according to the results, the effect of Reynolds in the case of large transition is small.

5. Acknowledgement

Support from Ship Research Institute of China (Grant Nos MAPT A pre research project), Mechatronics school Harbin Institute of Technology, Department of Motorcar Engineering Heilongjiang Institute of Technology and Key Laboratory of Hydrodynamics of China are gratefully acknowledged. The authors are grateful to Dr. Zhao xuezeng at HIT for discussions. A part of the computations was performed on Dawning-TC5000 system at Supercomputing Cetre, Shenzhen Institute of Advanced Technology, CAS, China.

References

[1] Chen H, Kandasamy S, Orszag S, et al (2003), Extended Boltzmann kinetic equation for turbulent flows. ***science*** 301: 635-638.
[2] Chen SY, Doolen GD (1998). Numerical simulation method for fluid flows. ***Annu. rev.Fluid Mech*** 30:330-365.
[3] Chen H,Filippova O,Hoch Jet al (2006). Numerical simulation method based on volumetric formulation. ***Physica A*** 363:159-168.
[4] Chen XP, ZHong CW, Yuan XL (2011). of cavitating bubble growth with largedensity ratio. ***Comput. Math. Appl***.62:3578-3585.
[5] Counsil JNN, Boulama KG (2012).Validating the URANS shear stress transport model for low -Reynolds-number external aerodynamics. ***Int. J. Num. Method Fluids*** 70:1412-1433.
[6] Estallo SI (2008). ***Comptational Gas Dynamics with the Numerical simulation method.*** PHD. Dissertation, Universidad de Zaragoza.
[7] Finck M, Hanel D, Wlokas (2007). Simulation of nasal flow by numerical simulation methods. ***Comput.Bio. Med.*** 38:740-750.
[8] Filippova O, Succi S, Mazzocco F, Arrighetti C, Bella G(2001). Multiscale numerical simulation schmes with turbulence modeling. ***J. Comput.Phys.*** 171: 813-830.
[9] Guo Z, Zheng C, Shi B（2002). An extrapolation method for boundary conditions in numerical simulation

methods. ***Phys Fluid*** 14(6): 2008-2011.

[10] d'Humieres D (2002). Multiple -relaxatin-time numerical simulation models in three dimensions. ***Phil. Trans. Roy.Soc.A*** 360: 438-452.

[11] Lallemand P, Luo L-S(2003). Theory of the numerical simulation method: Acoustic and thermal properties in two and three dimensions. ***Phys. Rev.E*** 68: 036706.

[12] Kam EWS, So RMC, Leung RCK (2007). Numerical Simulation Method of aeroacoustics and nonreflecting boundary conditions. ***AIAAJ.*** 45(7):1704-1713.

[13] Liu M, Chen XP, Premnath KN (2012). Comparative study of the large eddy simulations with the method using the wall-adapting local eddy viscosity and Vreman subgrid scale models. ***Chin. Phys.Lett.***29 (10):104706.

[14] Lallemand P, Luo LS (2003). Numerical Simulation Method for moving boundaries. ***J.Comput.Phys.*** 185:408-423.

[15] Premnath KN, Pattison MJ, Banerjee S (2009). Generalizied numerical simulation equation with forcing term for computation of wall-bounded turbulent flows.***Phys. Rev. E*** 79:026703.

[16] Rumsey CL, Spalart PR (2009). Turbulence model behavior in low Reynolds number regions of aerodynamic flow fields. ***AIAAJ.*** 47(4): 983-995.

[17] Scagliarini A, Biferale L, Sbragaglia M, Sugiyama K(2010). Numerical Simulation Method for thermal flows: Continuum linit and applications to compressible Rayleigh-Taylor systems. ***Phys Fluid*** 22: 055101.

[18] Shankar M, Sundar S(2009). Asymptotic analysis of extrapolation boundary conditions for NSM. ***Comput. Math. Appl.*** 57: 1315-1325.

[19] Spalart PR (2000). Strategies for turbulence modeling and simulations. ***Int.J.Heat Fluid Flow*** 21:256-266.

[20] Yu D, Mei R, Luo LS,Shyy W(2003). Viscous CD40 computations with the method of numerical simulation equation. ***Proc.Aerospace Sci.*** 39:330-368.